Climate Dynamics (2024) 62:3027–3046
https://doi.org/10.1007/s00382-023-07048-3

ORIGINAL ARTICLE

Decadal changes in the intraseasonal variability of intensity and location of East Asian polar-front jet around 2000 and associated mechanisms

Jingnan Yin[1,2] · Yaocun Zhang[2] · Daokai Xue[2] · Anning Huang[2] · Xueyuan Kuang[2]

Received: 17 May 2023 / Accepted: 25 November 2023 / Published online: 29 December 2023

Abstract

The East Asian jet stream is an important component of mid-high latitude circulation systems, and its intraseasonal oscillation plays a crucial role in the formation and development of persistent climate anomalies and extreme events over East Asia–Pacific region. This study examines the decadal changes in the intraseasonal variability (ISV) of the East Asian jet stream and investigates the possible reasons with reanalysis and observational datasets. It is found that the zonal winds over East Asia show notable ISV with a significant period of 10–25 days. The variance of 10–25-day filtered East Asian zonal winds exhibits a significant decrease around 2000, which is mainly contributed by the weakened ISV of westerlies within the key region of East Asian polar front jet (EAPJ). Further analysis reveals that the EAPJ experienced remarkable ISV changes in both intensity and location. The ISV of EAPJ intensity was weakened around 2000 due to decreased frequencies of both the extremely strong and weak cases, whereas the ISV of EAPJ location was evidently enhanced, with the southward shifts increased more than the northward ones. Along with the ISV increase (decrease) of EAPJ intensity (location), the dominant mode of EAPJ intraseasonal variation has changed from its intensity change to position shift since the year 2000. The decadal ISV changes and mode transition of EAPJ are closely associated with the modulation of lower-level large-scale circulation over Eurasia. The weakened ISV of meridional winds over Ural region after 2000 is favorable for an intraseasonal circulation pattern change from a continental-scale cyclonic anomalous pattern to a meridional dipole structure across the Eurasia in lower troposphere, resulting in regime shifts of East Asian temperature and its meridional gradient through temperature advection. The intraseasonal temperature gradient patterns display ISV changes parallel to those of EAPJ around 2000, indicating that the thermal anomalies are effective in leading to corresponding intensity and location variations of EAPJ via thermal wind relationship. Furthermore, the modulation of lower-level circulation is closely related to strengthened Arctic warming and weakened temperature variability over Barents sector after 2000, which may further be linked to sea ice reduction in the Barents Sea.

1 Introduction

The atmospheric circulation over mid-high latitudes in northern hemisphere consists of several large-scale systems, among which the East Asian upper-level jet stream is crucial for climate anomalies in East Asia. There are two separate jets over East Asia, referred to as the East Asian polar front jet (EAPJ) and subtropical jet (EASJ). The two jets are dominated by their intensity changes and latitudinal shifts on various time scales (e.g. Kuang and Zhang 2005; Zhang et al. 2006; Li and Zhang 2014; Luo and Zhang 2015; Xue and Zhang 2017; Yin and Zhang 2021). These jet variations have been reported to be closely associated with persistent weather and climate anomalies such as cold surges, extreme rainfalls and storm tracks over East Asia and Pacific region

✉ Yaocun Zhang
yczhang@nju.edu.cn

✉ Daokai Xue
dkxue@nju.edu.cn

[1] School of Naval Architecture and Ocean Engineering, Jiangsu University of Science and Technology, Zhenjiang 212100, China

[2] School of Atmospheric Sciences, Nanjing University, Nanjing 210023, China

(Robinson and Black 2005; Hong et al. 2009; Athanasiadis and Wallace 2010; Chen and Zhai 2014; Zhang et al. 2014), rendering a necessity to explore the characteristics and mechanisms of East Asian jet variations on different time scales.

The intraseasonal oscillation of jet streams has received particular attention in recent years, which has been investigated in terms of the strength fluctuation, north–south migration and east–west extension (Matthews and Kiladis 1999; Deng and Jiang 2011; Jaffe et al. 2011; Liao and Zhang 2013; Feldstein and Lee 2014; Song et al. 2016; Yao et al. 2018). For instance, during 1979–2007, totally 19 westward Pacific jet retraction events were identified by Jaffe et al. (2011) with a period of around 20 days. In particular, the intraseasonal oscillation of East Asian jet stream has been implicated in many researches on persistent weather events (Liao and Zhang 2013; Kuang et al. 2014; Yao et al. 2018; Shen et al. 2021). During the persistent southern China snowstorm in 2008 winter, the EASJ was gradually reinforced while the EAPJ was weakened as a whole, indicating an out-of-phase intensity variation of the two jets on intraseasonal time scale (Liao and Zhang 2013). Also, a 10–30-day oscillation of the zonal winds in the EASJ entrance was detected by Yao et al. (2018), which is associated with persistent rainfall anomalies near Yangtze River Basin and southwest China. Intraseasonal oscillation is also identified for the strength of East Asian trough (EAT) which is dynamically coupled with the East Asian jet stream, and significant cold (warm) anomalies, which can last for nearly 20 days, are consequently induced over East Asia (North America) due to the intraseasonal EAT variations (Song et al. 2016). These results imply the vital significance of exploring the intraseasonal oscillation of East Asian jet stream for better understanding persistent climate anomalies and extreme events.

Around the late 1990s to early 2000s, many different climate extremes underwent pronounced decadal transitions, involving heavy snowfalls, intense precipitations and low temperature extremes (Woo et al. 2012; Kuang et al. 2016; Cheng et al. 2020; Zhou et al. 2021). In view of the intimate association between intraseasonal oscillation of the jets and extreme events, it would be of great significance to investigate the characteristics and mechanisms of the decadal change in intraseasonal jet variation (if any) for better understanding the decadal changes in various extreme events. In fact, pronounced changes in the intraseasonal oscillation of East Asian jet stream have been identified and proven to play a vital role in the decadal shifts of extreme events in some previous studies. Kuang et al. (2016) revealed that the record-breaking low temperature events tended to occur over southern China in the 1990s accompanied by extremely intensified EAPJ that favors cold air mass break out and southward invasion into low latitudes, but were mostly located over northern China in the 2000s in conjunction with the northward shift of EASJ that accumulates cold air mass in midlatitudes. Huang et al. (2015) also found that the frequency of spring persistent rainfall has decreased since the late 1990s, which is contributed by the collocation of weakened EASJ and strengthened EAPJ. Therefore, whether there are certain decadal changes in the intraseasonal oscillation of East Asian upper-level jets deserves further investigation; if it does exist, it would help provide a new perspective to interpret and predict the decadal changes in extreme events and persistent climate anomalies.

The decadal changes in the East Asian upper-level jets actually have been unveiled by previous studies, but these studies only considered their seasonal mean states (Huang et al. 2019; Yin and Ting 2021; Zhou et al. 2021). According to the results of Yin and Zhang (2021), the intensity of winter-averaged EAPJ and EASJ showed an out-of-phase decadal change around 1985, whereas the two jets moved toward each other after 1999. Such decadal changes of the jets can serve as a favorable circulation background of climate extremes (Woo et al. 2012; Kuang et al. 2016; Song and Wu 2018; Zhou et al. 2021), and further implicate corresponding differences in the intraseasonal oscillation of East Asian jet stream. In fact, it has been claimed that much of the interdecadal poleward shift of the jets can be interpreted by the frequency changes in the intraseasonal patterns of zonal-mean westerlies (Lee and Feldstein 2013; Feldstein and Lee 2014). This is conceivable as lower-frequency evolution can commonly be deemed as a representative of higher-frequency disturbances. Similar relationships between lower- and higher-frequency variations can also be identified in temperature and rainfall anomalies. In northeast Asia, the interannual variability of temperature maximum and the frequency of high temperature days increased abruptly under the background of warming summer mean temperature around the early to mid-1990s (Wei and Chen 2011; Chen and Lu 2014; Chen et al. 2021). Also, both the interannual and intraseasonal variability of summer rainfall over southern China displayed a coherent enhancement with its wintertime mean state around the early 1990s (Chen et al. 2015, 2017; Cheng et al. 2020). These evidences imply that change in lower-frequency state can be accompanied by change in the occurrence of in-phase higher-frequency oscillations. It can thus be inferred that the effect of lower-frequency regulation primarily manifests as the decadal changes in the variability (i.e. variance or standard deviation) of higher-frequency fluctuations. Hence, the present study mainly examines the decadal changes in the intraseasonal variability (ISV; i.e. variability of intraseasonal oscillation) of the East Asian jet stream in winter and further indicates the underlying mechanisms.

Based on previous studies, the mechanisms of jet variations can be generally probed with respect to both the

internal dynamics and external forcings. Positive feedbacks between transient eddy and basic flow contribute much to the acceleration of upper-level westerlies (Hoskins et al. 1983; Luo and Zhang 2015; Wang and Zhang 2015; Xue and Zhang 2017). Thermal forcings from Tibetan Plateau, sea surface temperature, snow cover and sea ice extent are all critical conduciveness to the jet changes on various time scales (Luo and Zhang 2015; Huang et al. 2017, 2019; Yin and Zhang 2021). In particular, we note that Arctic sea ice has reduced remarkably alongside the increasingly prominent Arctic amplification since the late 1990s (e.g. Serreze et al. 2009; Wu et al. 2013; Cohen et al. 2014; Screen 2014), and some evidences have been presented concerning the changes in jet variability owing to the Arctic amplification and sea ice reduction (Francis and Vavrus 2012, 2015; Woollings and Blackburn 2012; Feldstein and Lee 2014; Barnes and Simpson 2017; Ronalds et al. 2018; Xu et al. 2018). Therefore, the possible contribution of Arctic conditions to decadal changes in the ISV of East Asian jet stream is taken into consideration in this work.

To sum up, previous studies have implied certain alterations in the ISV of East Asian jet stream on interdecadal time scale. It can be of great significance to excavate and expatiate the feature and mechanism of the decadal ISV changes in jets for better comprehending and predicting the decadal variations of persistence climate anomalies and extreme events. However, it is rather unclear at what time, in what forms and for what reasons the ISV of East Asian jet stream undergoes decadal changes. These issues will be addressed in the current study. The rest of the paper is organized as follows. Section 2 introduces the datasets and methods. The decadal changes in the ISV of East Asian jets in terms of the intensity and location are expatiated in Sect. 3. Section 4 further investigates the possible reasons for the decadal ISV changes of the jets from a thermal perspective. Summary and discussion are provided in Sect. 5.

2 Data and method

The daily mean zonal and meridional winds, geopotential height and air temperature used in this study are derived from the National Centers for Environmental Prediction-National Center for Atmospheric Research (NCEP-NCAR) reanalysis data (Kalnay et al. 1996) with a horizontal resolution of 2.5° × 2.5° during 1979–2020. The monthly sea ice concentration (SIC) data from the Met Office Hadley Center with a horizontal resolution of 1° × 1° (Rayner et al. 2003) from 1979 to 2020 are also utilized. The global monthly SST used in this study are from National Oceanic and Atmospheric Administration (NOAA) Extended Reconstructed SST, version 5 (ERSSTv5; Huang et al 2017).

The time period involved in this study is 41 winters from 1979 to 2019. Winter is defined from December, February to January (DJF), like Dec 1979 and Jan-Feb 1980 means the winter of 1979. The power spectrum analysis (Gilman et al. 1963) is used to determine the dominant periods of the intraseasonal oscillation of East Asian jet stream. The empirical orthogonal function (EOF) and probability distribution function (PDF) are employed to examine the leading modes of the intraseasonal jet variation and its frequency distribution, respectively. Statistical regression, correlation and composite analyses are also adopted in the present study. The Lanzcos band-pass filter (Duchon 1979) is applied to separate the intraseasonal components from daily anomalies, and a 9-year low-pass filter is also employed to display interdecadal evolution. The Student's t test is used for the significance test of regression and composite anomalies. The ISV of East Asian jet stream is measured with the variance of intraseasonal westerlies over East Asia in each year, and the significance of the decadal ISV change is assessed by the F test. Effective degree of freedom has been taken into consideration in these significance tests.

3 Decadal transition in ISV of EAPJ intensity around 2000

The variance of 10–90-day filtered zonal winds averaged over East Asia (20°–60° N, 70°–120° E) in each winter is presented in Fig. 1a to detect the decadal changes in the intraseasonal variability (ISV) of East Asian jet stream variation. With the normalized variance transited from a positive to negative phase around 2000, the ISV of East Asian westerlies weakened abruptly at a confidence level of 95% according to the F test. To further identify the dominant intraseasonal period of East Asian zonal winds, Fig. 1b enumerates the significant periods during 1979–2020 by conducting power spectrum analysis on the intraseaonal (10–90-day) westerlies averaged over East Asia in each year. It turns out that the vast majority of periods above 99% confidence level (red star) are concentrated in the 10–25-day band. Within this band, there are nearly 26% of the total years surpassing the 99% confidence level (10.5 years for each period on average), whereas few years can reach this confidence level beyond this band (red line). Note that the significant periods shorter than 10 days are spurious signals that are inevitable due to the limitation of filtering method. The variance of 10–25-day filtered zonal winds over East Asia also manifests significant decrease around 2000 (Fig. 1a). The ratio of the variance of East Asian-mean zonal wind filtered in 10–25-day period to that filtered in 10–90-day period is over 66%, which indicates that the 10–25-day oscillation contributes about two-thirds of the total intraseasonal variance. The above results suggest that the intraseasonal oscillation

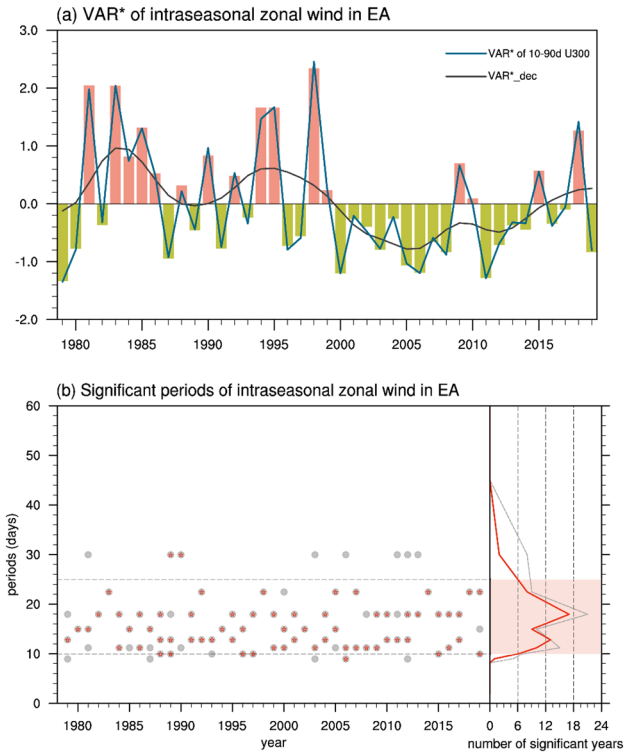

Fig. 1 **a** Normalized variance of the 10–90-day (blue line) and 10–25-day (bar) filtered 300-hPa zonal wind regionally averaged over East Asia (20°–60° N, 70°–120° E) in each winter of 1979–2019. Black curve in **a** represents the decadal component of the blue polyline derived with 9-year low-pass filter. **b** Significant periods exceeding the confidence level of 90% (grey dot) and 99% (red star) in each year. The two horizontal dotted lines in the left panel of **b** indicate the periods of 10 and 25 days, respectively. The grey (red) line in the right panel of **b** represents the number of years at 90% (99%) significance level for different periods

of East Asian zonal winds is dominated by the period of 10–25 days. Hereafter, a 10–25-day filter has been applied to all daily variables before further statistical analyses.

On this basis, to further figure out which jet dominates the East Asian wind variations and ISV changes, Fig. 2 presents the 300-hPa intraseasonal zonal wind anomalies regressed against the normalized series of regionally averaged westerlies over East Asia. It is indicated that the acceleration of East Asian zonal winds is mainly contingent on the anomalous westerlies along the key regions of East Asian polar front jet (EAPJ; 40°–60° N, 70°–120° E) and East Asian subtropical jet (EASJ; 25°–35° N, 75°–105° E). The normalized intraseasonal zonal winds averaged in these two regions are then identified as the intensity index of EAPJ (EAPJI_int) and EASJ (EAPJI_int) for further examining their variance evolutions. Different from that no evident decadal change is displayed in the normalized series of EASJI_int variance (Fig. 2c), pronounced weakening is observed in the evolution of EAPJI_int variance around 2000 (Fig. 2b). Additionally, a correlation of 0.67 is detected between the variance series of zonal winds in EAPJ key region (Fig. 2b) and that across East Asia (Fig. 1a). It is therefore suggested that the ISV weakening of EAPJ intensity takes a major responsibility for the variance drop of East Asian zonal winds around 2000.

Previous studies have suggested that the variability/variance is interrelated with the occurrence frequency of extreme events; larger variability commonly points to higher probability of extreme case occurrences (Ito et al. 2013; Chen et al. 2021; You and Ting 2021). We thereupon examined the changes in extreme intensity frequency of EAPJ from the earlier (1979–1999; P1) to recent (2000–2019; P2) subperiod to better comprehend the ISV changes of EAPJ intensity. As demonstrated in Fig. 2b, the 10% strongest (the most positive EAPJI_int larger than 90th percentile; red line), the 10% weakest (the most negative EAPJI_int less than 10th percentile; green line) EAPJ intensity frequencies as well as their summation (yellow line) all show remarkable decrease around 2000. Here the extreme frequency refers to ratio of 10% strongest (weakest) days to a winter (90 days), and the 10% strongest days represent the days with values larger than the 10th percentile of the entire period. Moreover, the summation series is highly correlated with the variance of EAPJI_int (Fig. 1a) at 0.96. The decadal changes in extreme intensity frequencies indicate that the variance of EAPJ intensity is declined due to the decrease of both the extremely strong and weak days, which is reconfirmed by the comparison between frequency distributions of EAPJI_int in P1 and P2. As shown in Fig. 3a, P2 shows a higher and narrower distribution than P1, with both the strong and weak tails shifting towards the center. Positive differences are observed in the middle of the horizontal axis where small absolute values reside, and negative differences are seen at the ends in which large absolute values lie (black line). The absolute value of EAPJI_int that separates the positive and negative differences is approximately 1.2 standard deviation (std; black line). To more intuitively gauge to what extent the extreme (non-extreme) days decreased (increased) in P2, Fig. 3b provides the percentage frequency differences between EAPJI_int in P2 and P1 within different thresholds. Generally, with the absolute values of EAPJI_int decreasing from over 3 std to 0, the frequency differences keep rising from negative to positive. Particularly, the number of extreme days with absolute values larger than 3 std has reduced by an enormous ratio of over 80%. The frequencies of absolute values less than 1.2 std increased by 6% on the whole, whilst those more than 1.2 std decreased more notably by 16%.

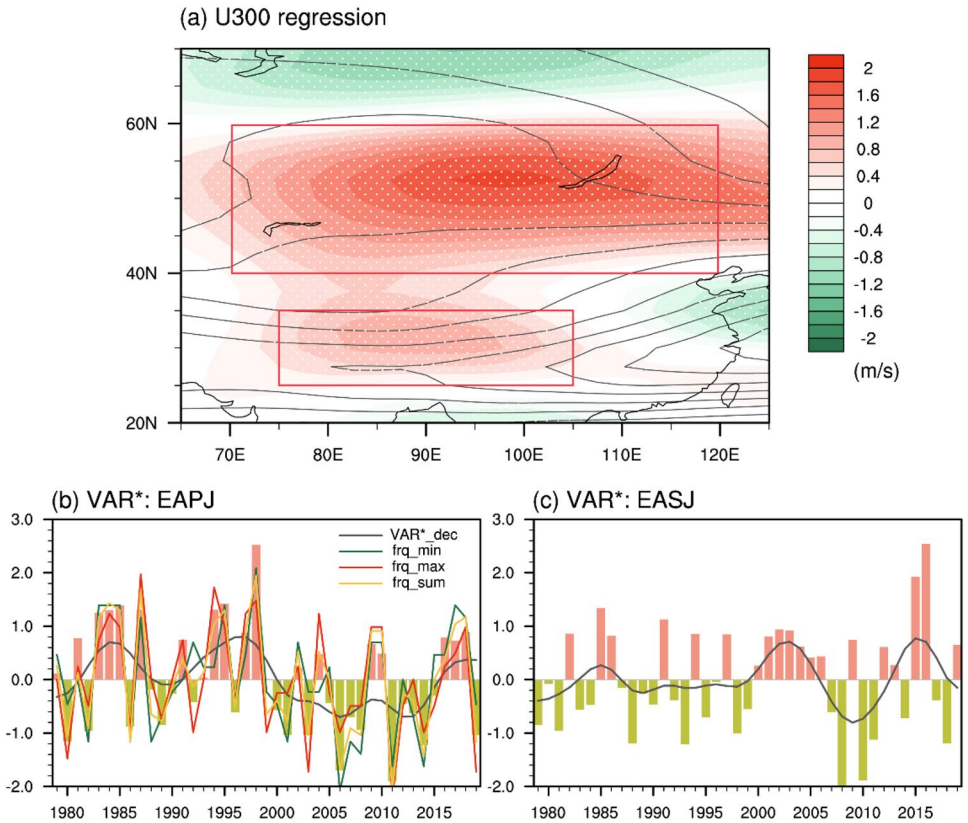

Fig. 2 **a** The 10–25-day filtered 300-hPa zonal wind anomalies (shading) regressed onto the normalized time series of its regional mean over East Asia (20°–60° N, 70°–120° E). Contours in **a** denote the climatological 300-hPa zonal wind in winter. **b** The normalized variance of the intensity index of EAPJ (EAPJI_int). **c** Same as **b**, but for intensity index of EASJ (EASJI_int). Red rectangles in **a** outline the key regions for definition of EAPJI_int and EASJI_int. White dots in **a** indicate the anomalies at 99% significance level. Red, green and yellow lines in **b** represent the normalized frequencies of 10% largest EAPJI_int, 10% smallest EAPJI_int and their summation. Black curves in **b** and **c** represent the decadal components of the variance of EAPJ and EASJ (bar)

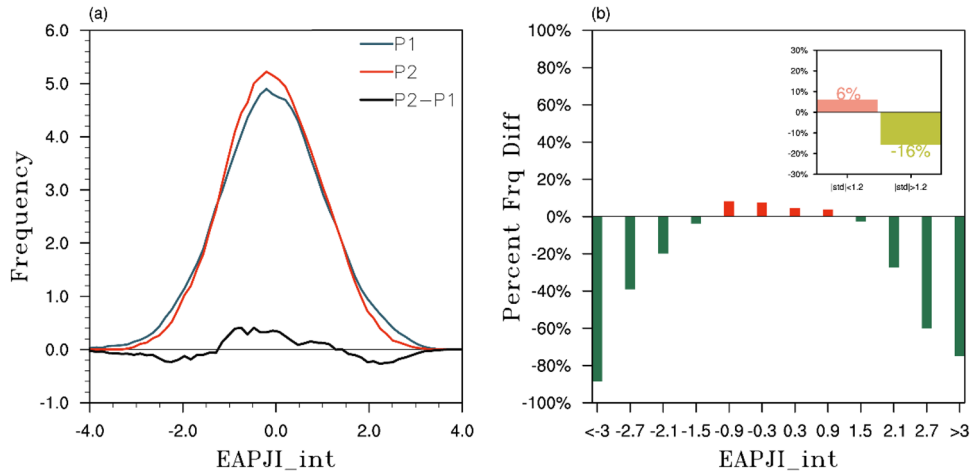

Fig. 3 **a** Frequency distribution of EAPJI_int during 1979–1999 (P1; blue line) and 2000–2019 (P2; red line) as well as their difference (black line). **b** The percentage of the frequency difference of EAPJI_int between P2 and P1 (black line in **a**) to the frequency distribution in P1 (blue line in **a**) for different thresholds. Bin width of each threshold in **b** is 0.6 standard deviation (std). The frequency difference percentage for thresholds of absolute values larger (green bar) and less (red bar) than 1.2 std is further counted in the small plot in the upper-right corner of **b**

4 Decadal transition in ISV of EAPJ location around 2000

The intensity change of EAPJ is reminiscent of its leading mode. Generally speaking, the jet variation is mostly manifested as its intensity change or location shift. It is thus reasonably speculated that the ISV reduction of EAPJ intensity change might collocate with a dominant mode transition of EAPJ. This speculation is testified with Empirical orthogonal function (EOF) analysis of the

normalized intraseasonal zonal winds in EAPJ key region before and after 2000 (Fig. 4a, b). The first mode of EOF analysis in P1 (EOF1-P1) manifests consistent zonal wind anomalies across EAPJ key region, reflecting the change of EAPJ intensity (Fig. 4a). EOF1 in P2 (EOF1-P2), by contrast, exhibits a meridional dipole structure centered at around latitude 50° N, representing the north–south shift of EAPJ location. It means that accompanied by the ISV decrease of EAPJ intensity, the dominant mode of EAPJ intraseasonal variation has switched from its intensity change to location shift around 2000.

Inspired by the leading mode transition of EAPJ in Fig. 4, we anticipated a high probability that the ISV of jet location shift also experienced decadal change around 2000. To verify this anticipation, a location index of EAPJ (EAPJI_loc) is defined as the difference between normalized intraseasonal zonal winds averaged over (50°–60° N, 70°–120° E) and (40°–50° N, 70°–120° E), based on the spatial distribution of EOF1-P2 (Fig. 4b). A positive value of EAPJI_loc indicates the northward shift of EAPJ. The variance of EAPJI_loc in each year is presented in Fig. 5, and abrupt variance increase can be observed around 2000 (black curve), suggesting a robust ISV strengthening of the position migration of EAPJ.

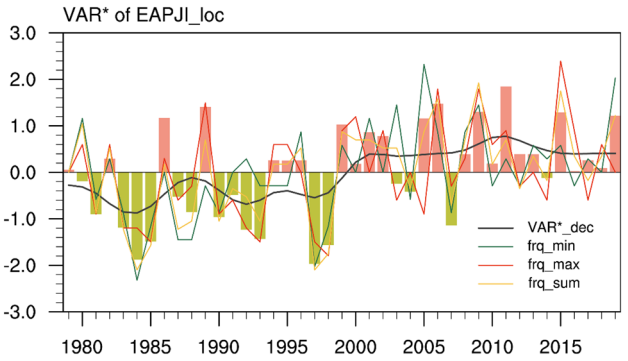

Fig. 5 Same as Fig. 2b, but for EAPJI_loc

The ISV strengthening of EAPJ location can also be expounded by virtue of the contributions of both the extremely southward and northward shifts of EAPJ axis. The frequencies of 10% southward (the most positive EPAJI_loc larger than 90th percentile; red line) and 10% northward (the most negative EAPJI_loc less than 10th percentile; green line) migrations both increased around 2000, and their summation series (yellow line) has a correlation of 0.89

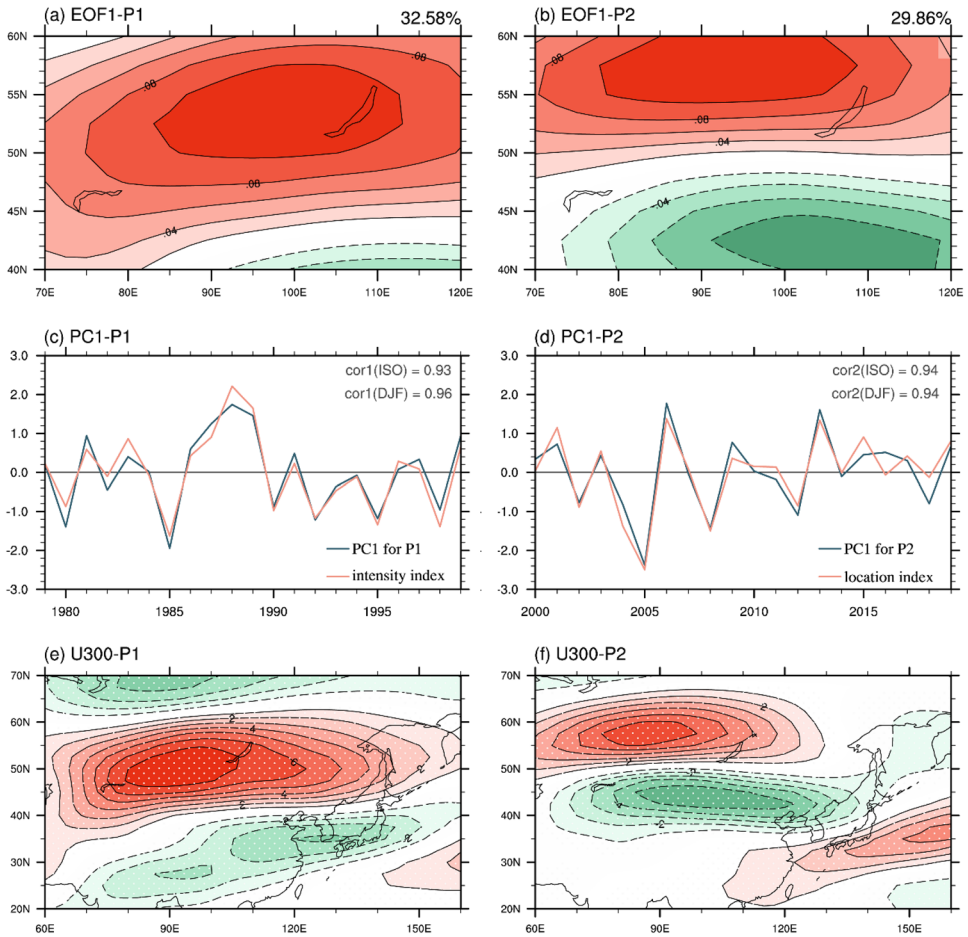

Fig. 4 The first mode of EOF analysis (EOF1) of 300-hPa 10–25-day filtered zonal wind in EAPJ key region (40°–60° N, 70°–120° E) in **a** P1 and **b** P2, respectively. Percentage at the upper-right corner of **a** and **b** denotes the explained variance. **c** Comparison between normalized series of winter-time-averaged first principle component in P1 (PC1-P1; blue line) and EAPJI_int (pink line). Texts at the top right corner of **c** represent correlation coefficients between intraseasonal and annual component of PC1-P1 and EAPJI_int. **d** Same as **c**, but between first principle component in P2 (PC1-P2) and EAPJI_loc. **e** Composite anomalies of intraseasonal zonal wind (m/s) at 300 hPa between positive (> 1.2 std) and negative (< − 1.2 std) EAPJI_int in P1. **f** Same as **e**, but for EAPJI_loc in P2. Anomalies significant at 99% confidence level are dotted in **e** and **f**

with the variance of EAPJI_loc. The collaborated contributions of extreme northward and southward displacements of EAPJ are also supported by the frequency distributions of EAPJI_loc in the two subperiods (Fig. 6a). A lower and wider frequency distribution is formed in P2 (red line), generating negative frequency differences in the middle of the horizontal axis and positive differences at the ends (black line). As can be seen in the percentage frequency differences (Fig. 6b), the threshold between positive and negative differences is also around ± 1.2 std, and frequencies with absolute values more (less) than 1.2 std generally increased (decreased) by around 20%. It is worth noting, though, discernible asymmetry occurs between the increments of strong northward (> 1.2 std) and southward shifts (< − 1.2 std) despite their consistent growth trend (Fig. 6b). In contrast to the coherent increase of strong southward shifts, the frequencies of northward shifts only increase within thresholds from 1.2 to 2.7 std, whilst extreme northward shifts over 3 std are considerably reduced by 40%. As a result, the frequencies of southward shifts have increased (by 23.6%) more than those of northward ones have increased (by 16.4%) in P2. The more frequently occurring extreme southward shifts are consistent with the southward migration of EAPJ climatological location, and a positive feedback may work between the two. On the one hand, in light of the relationship between lower and higher frequency oscillations, the increased extreme southward shifts implicate a slow southward migration in winter mean state of EAPJ. On the other hand, the southward migrated winter mean state in turn favors the more frequent occurrences of extreme southward shifts by skewing the probability distribution of EAPJI_int to southward tails.

In a nutshell, the ISV of EAPJ intensity (location) has weakened (strengthened) significantly since the beginning of twenty-first century, with the dominant mode of EAPJ switched from its intensity change to location migration. This is reasonable because the meridional dipole pattern in EOF1-P2 show reversed anomalies on the north and south side of EAPJ, which actually counteract each other. Such counteraction prejudices the overall westerly change in EAPJ key region, and thus damps the ISV of EAPJ intensity. In contrast, such dipole pattern in EOF1-P2 favors the amplification of EAPJ's meridional oscillation by increasing the zonal wind difference between the north and south of EAPJ axis, and thereby strengthens the ISV of its location shift.

To verify the linkage between the ISV change and mode transition of EAPJ, we compare the EAPJI_int and EAPJI_loc with the first principle component in the earlier (PC1-P1) and recent (PC1-P2) subperiod, respectively (Fig. 4c, d). It turns out that PC1-P1 (PC1-P2) is highly correlated with EAPJI_int (EAPJI_loc) at a coefficient of 0.93 (0.94) on intraseasonal time scale. In addition, as seen in Fig. 4e, f, the composited differences between 300-hPa intraseasonal zonal winds with strong positive and negative EAPJI_int (EAPJI_loc) in P1 (P2) can precisely capture the primary feature of EOF1-P1 (EOF1-P2). Also, both composites are spatially correlated with the EOF1 mode in corresponding subperiod at 0.95. That is, the intensity and location indices of EAPJ, whose ISVs show significant decadal changes, can accurately reflect the major patterns of EAPJ variation in P1 and P2, respectively. It is thus implied that the decadal changes in the ISV of EAPJ intensity and location might provide a new perspective for understanding its mode transition around 2000. In the next section, EAPJI_int and EAPJI_loc will be utilized to describe the major patterns of EAPJ and the associated circulation anomalies in P1 and P2, respectively, so as to investigate the possible reasons for the ISV changes and mode transition of EAPJ.

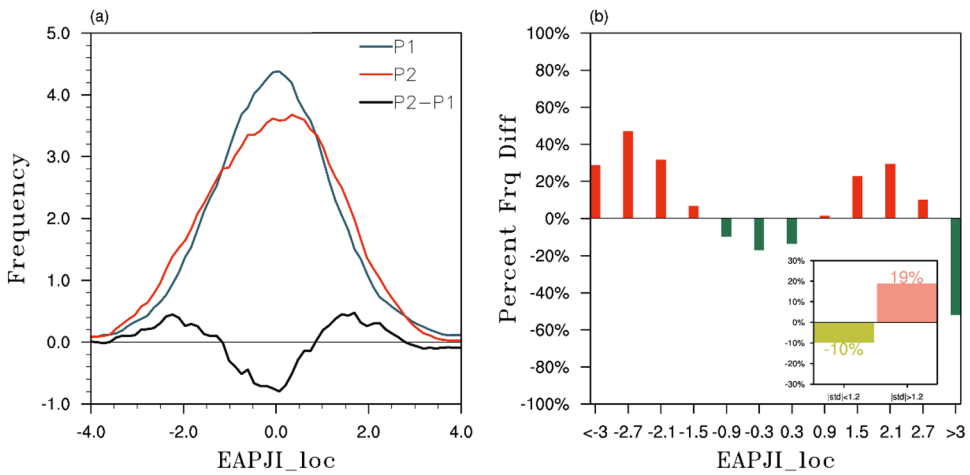

Fig. 6 Same as Fig. 3, but for EAPJI_loc

5 Possible reasons for the decadal changes in the ISV of EAPJ

From a thermodynamic perspective, changes in upper-level jets can be explained by anomalies of meridional temperature gradients below the westerlies based on thermal wind relation, through which the anomalous thermal signals can be transported from the surface to upper troposphere and exert forcing on zonal winds. Thermal anomalies are tightly associated with circulation regimes, so we first display the lower-level intraseasonal circulation patterns related to the dominant mode of EAPJ variation in the two subperiods (Fig. 7a, b). The lower-level circulation patterns are represented by geopotential height and wind fields at 850 hPa, and remarkable distinctions are observed between corresponding anomaly fields in P1 and P2. The whole Eurasian continent is occupied by a strong cyclonic anomaly in P1, whereas a meridional dipole structure is formed in P2 with elongated cyclonic and anticyclonic anomalies covering mid-high latitude and subtropical Eurasia, respectively. Accordingly, the relevant intraseasonal meridional wind anomalies also display significant differences. A pair of zonal dipole anomaly centers of meridional winds occurs over the mid-high latitude Eurasia in both P1 and P2 (shading in Fig. 7a, b), but the amplitude of the anomaly centers is much weaker in P2 than in P1. To clarify such amplitude weakening, the difference between the absolute values of meridional wind anomalies in P2 (Fig. 7b) and P1 (Fig. 7a) is further presented in Fig. 7c. It turns out that the most remarkable difference occurs around the Ural region (40°–60° N, 45°–65° E; red rectangle in Fig. 7c) manifesting as significant decrements, which hints an ISV decrease of Ural-meridional winds from P1 to P2.

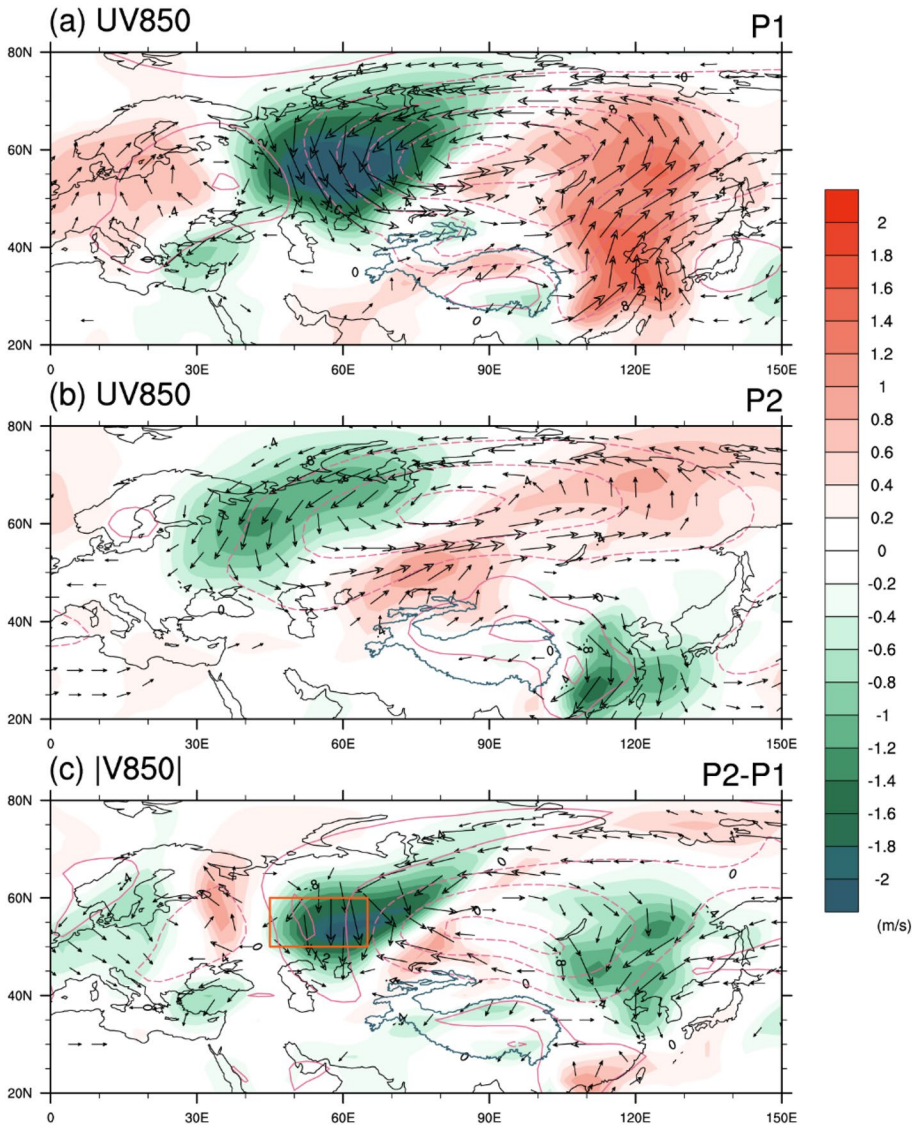

Fig. 7 Composite differences of intraseasonal wind (vector), its meridional component (shading; m/s) and geopotential height (contour; gpm) at 850 hPa between days with positive (> 1.2 std) and negative (< − 1.2 std) **a** EAPJI_int in P1 and **b** EAPJI_loc in P2. **c** Difference of absolute values of the meridional winds in **b** and **a**. Only meridional wind anomalies exceeding 99% confidence level are shaded. Wind vectors with amplitude less than 0.5 m/s are omitted. Tibetan Plateau (TP) boundary is outlined in dark blue

To verify such ISV decrease of Ural-merioindal winds, the normalized variance of the intraseasonal meridional winds averaged over the Ural region is presented in Fig. 8a. As expected, the variance displays a significant reduction around 2000, affirming the ISV weakening of Ural-meridional winds. This weakened ISV can also be owed to the frequency changes in the meridional wind extrema over Ural region. The 10% extreme southerly winds (the most positive Ural-meridional wind larger than 90th percentile; red line) and 10% northerly winds (the most negative Ural-meridional wind less than 10th percentile; green line) as well as their summation (yellow line) all decreased around 2000 (red and green lines in Fig. 8a). The total extremum frequency is highly correlated with the Ural-meridional wind variance

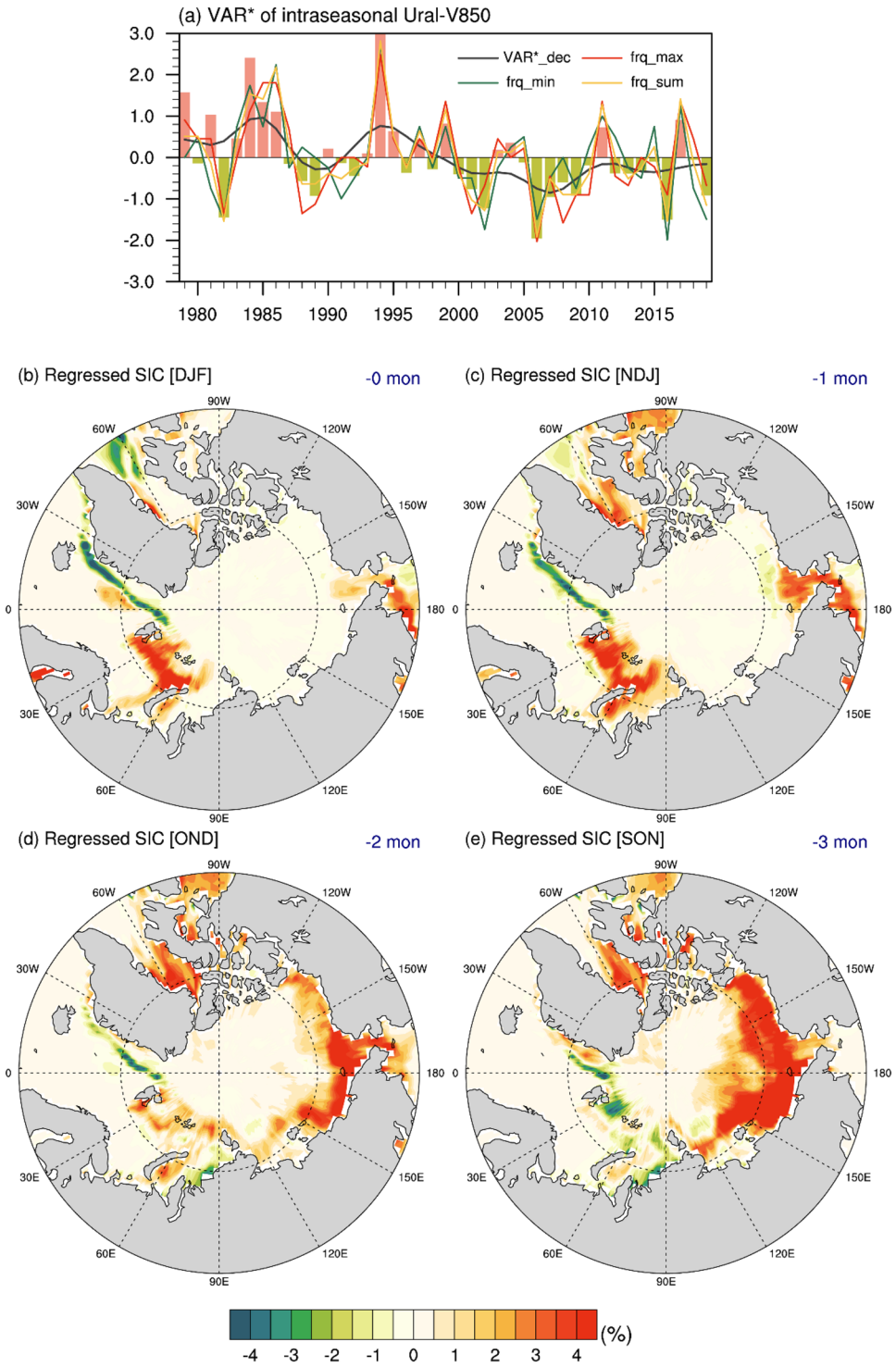

Fig. 8 **a** Same as Fig. 2b, but for 850-hPa intraseasonal meridional winds averaged over the Ural region (50°-60°N, 45°-65°E). Sea ice concentration (SIC) anomalies in **b** DJF, **c** NDJ, **d** OND and **e** SON regressed against the normalized summation series of 10% extreme values in DJF (yellow line in **a**). Texts at the top-right corner of **b–e** represent the leading months of SIC anomalies

at a coefficient of 0.91, validating that there exists compact interrelation between the variance and extreme frequency of Ural-mean meridional wind series.

The ISV decrease of Ural-meridional winds can be construed as an upstream trigger of the consequent large-scale circulation modulation over Eurasia. In P1, because the ISV of Ural-meridional winds is larger, cold air from the Arctic can intrude deep into southern Eurasia and gradually turn into westerlies, acting to excite a strong cyclonic anomaly center which can override the whole Eurasian continent (Fig. 7a). As a rule, when westerlies pass through the northern flank of Tibetan Plateau (TP), they are apt to transform into northerly winds along the eastern TP flank due to the dynamic forcing of TP to detour the flow, favoring the formation of an anticyclonic anomaly over the Plateau. As can be seen in Fig. 7a, the anomalous westerlies at the southern flank of the cyclonic anomaly can reach around 35°N in P1, south of the northern TP periphery. As a result, the anticyclonic anomaly over TP shrink to Southern Tibet, and the anomalous circulation pattern in Eurasia is mainly governed by the strong cyclonic anomaly generally covering the whole continent. Under this circumstance, only weak northerly winds occur along eastern TP flank, and thus most southerly flows from lower latitudes are allowed into East Asian landmass and converge with the eastern peripheral winds of the cyclonic anomaly, forming strong southerly winds over East Asia.

Instead in P2, due to the weakened Ural-meridional wind ISV, the northerly winds over the Ural region can only reach latitudes of around 50° N, thus narrowing down the previous cyclonic anomaly to the northern Eurasian region. The westerlies at the southern flank of the cyclonic anomaly are located right at the northern TP flank in P2. Therefore, owing to the detouring effects of TP, the westerlies bifurcate with one branch transformed into southerly winds along the cyclonic anomaly and another branch shifted as northerly winds along the eastern TP flank. Hence, obvious northerly winds are observed over southern East Asia in P2 (Fig. 7b). As a result, a meridional dipole structure of geopotential height anomalies is formed in P2.

On the whole, by virtue of modulating the circulation pattern in Eurasian lower troposphere, the weakened ISV of meridional winds in Ural region arouses the intensity-to-location mode transition of EAPJ, which actually comes down to the ISV decrease in intensity change, and the ISV increase in location shift at the same time. This viewpoint is corroborated by the high correlation coefficients between the decadal variance of Ural-meridional winds and that of both the EAPJI_int (0.78) and EAPJI_loc (− 0.85; Table 1). Moreover, the variance of EAPJI_int and EAPJI_loc is also negatively intercorrelated at − 0.54, and their decadal components have a higher correlation coefficient of − 0.73 (Table 1). This negative correlation is understandable since the intensity and location variation constitute the first two leading modes of EPAJ. Hence when one mode occurs less frequently, the other one naturally tends to occur more frequently as a substitute.

The decadal changes in lower-level circulation patterns further lead to salient differences in air temperature and its meridional gradients, mainly through the contribution of horizontal temperature advection (contour in Fig. 9a, b). Specifically, In P1, the most conspicuous feature of temperature anomalies is the significant negative anomalies over Siberia and positive anomalies over East Asia (shading in Fig. 9a). These temperature anomalies are induced by both zonal and meridional temperature advections (Fig. 10a, c), which contribute to different parts of the anomalies. The northern part of Siberian negative anomalies is contributed by easterly advection along northern Russia (Fig. 10a), while the southern part is induced owing to the northeasterlies on the northwest of the cyclonic anomaly blowing cool air from the Arctic toward mid-high latitude Eurasia (Fig. 10c). In comparison, positive anomalies in East Asia are generated differently. The western part of the positive anomalies is mainly induced by westerly advection along the southern flank of the anticyclonic anomaly (Fig. 10a), whereas the eastern part is aroused due to the southerlies on the southeast of the cyclonic anomaly carrying warm air from lower latitudes (Fig. 10c). As a result of such anomalous temperature distribution, significant negative temperature gradient

Table 1 Cross correlations among the mean and variance of Barents-temperature, variance of Ural-meridional winds, and variance of EAPJI_int and EAPJI_loc

	Barents-T mean	Barents-T variance	Ural-V850 variance	EAPJI_int variance	EAPJI_loc variance
Barents-T mean	–	− 0. 87*	− 0.69*	− 0.53	0.86*
Barents-T variance		–	0.79*	0.56	− 0.87*
Ural-V850 variance			–	0.78*	− 0.85*
EAPJI_int variance				–	− 0.73*
EAPJI_loc variance					–

All coefficients exceed 90% confidence level, and coefficients with a star exceed 95% confidence level

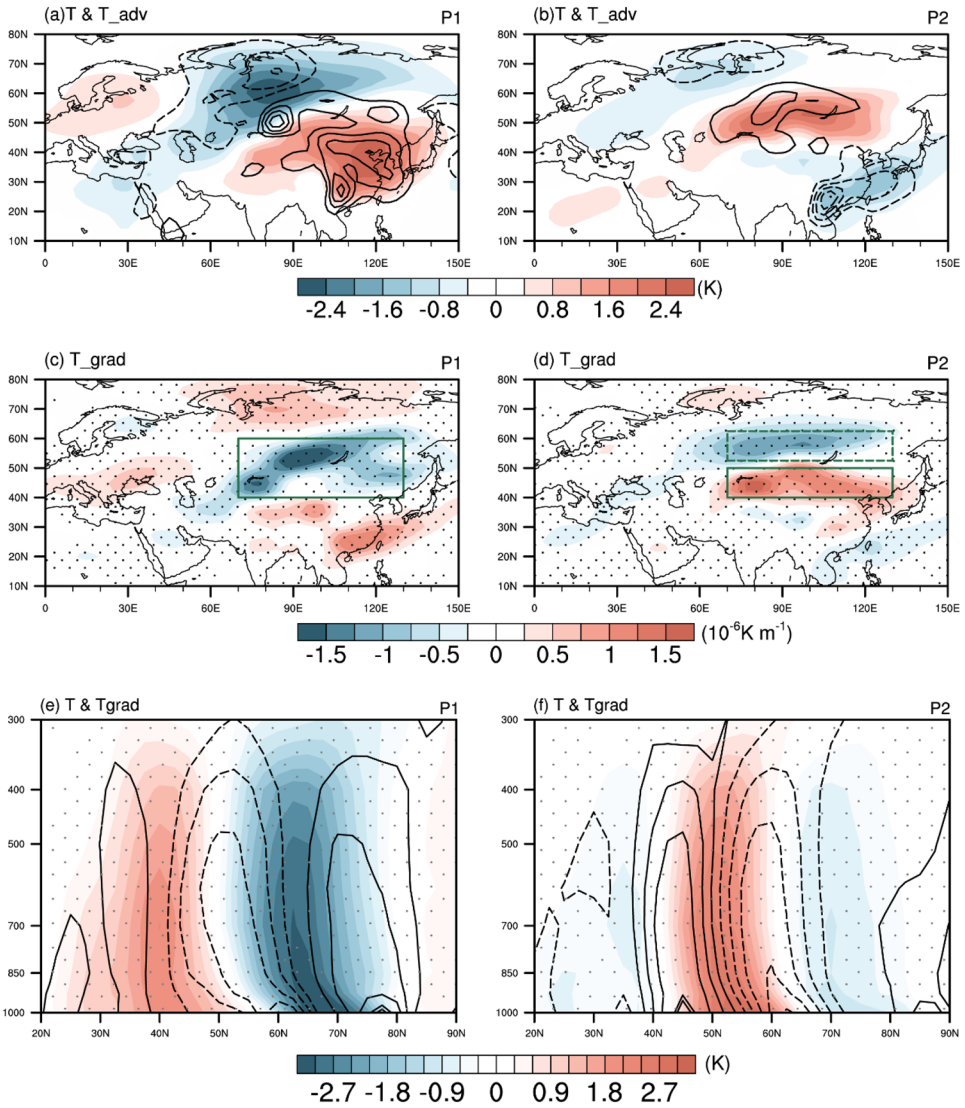

Fig. 9 Composite differences of intraseasonal air temperature (shading) and temperature advection (contour; K/day) at 850 hPa between days with positive (> 1.2 std) and negative (< − 1.2 std) **a** EAPJI_int in P1 and **b** EAPJI_loc in P2. Only temperature anomalies exceeding 99% confidence level are presented. **c**, **d** Same as **a**, **b**, but for meridional temperature gradient (contour). Dots in **c** and **d** indicate temperature gradient anomalies significant at 99% confidence level. Rectangles outline the key areas for definition of meridional temperature gradient indices (MTGI). **e. f** Same as **a**, **b**, but for (70°–120° E) zonal mean intraseasonal air temperature (shading) and its meridional gradients (contour; 10^{-6}Km^{-1}). Only temperature anomalies exceeding 99% confidence level are presented. Dots indicate temperature gradient anomalies significant at 99% confidence level

anomalies occur between the cold and warm centers around the latitude of 50° N (Fig. 9c). Such thermal anomalies can extent toward the upper troposphere with a quasi-barotropic structure particularly from 850 hPa to near 300 hPa, as is demonstrated by the vertical section of temperature (shading) and its meridional gradients (contour) in Fig. 9e. The vertically accumulated negative temperature gradient anomalies around 50°N contribute to accelerating the EAPJ through thermal wind theorem.

By contrast, the thermal conditions in P2 are quite different. A "warm-cold-warm" triple anomalous pattern forms over the Eurasia (shading in Fig. 9b). Similarly, both the zonal and meridional advection make notable contributions. By comparing the zonal and meridional advections in Fig. 10b, d, it is found that the warm anomalies over Lake Baikal are contributed by the advection of peripheral southwesterly winds of the cyclonic anomaly. Whereas the cold anomalies in southeastern coast China are generally attributed to the northerly advection at the eastern periphery of anticyclonic anomaly, with a supplementary contribution of the easterly advection in South China. Such triple anomalous temperature structure in P2 therewith leads to negative and positive temperature gradient anomalies on the north and south of 50°N. These thermal anomalies also extend till the upper troposphere with an equivalent-barotropic structure (Fig. 9f) and favor the northward migration of EAPJ according to the thermal wind theorem. Note that the temperature anomalies tilt southward below 850 hPa especially within 60°–75° N (50°–60° N) in P1 (P2). The southward tilting structure might arise from the large baroclinicity in lower troposphere over mid-to-high latitudes, which can be validated by the northward tilting anomalous geopotential height in those regions (figure not shown; Kosaka and Nakamura 2006; Tanaka et al. 2016; Hu et al. 2018; Li et al. 2020).

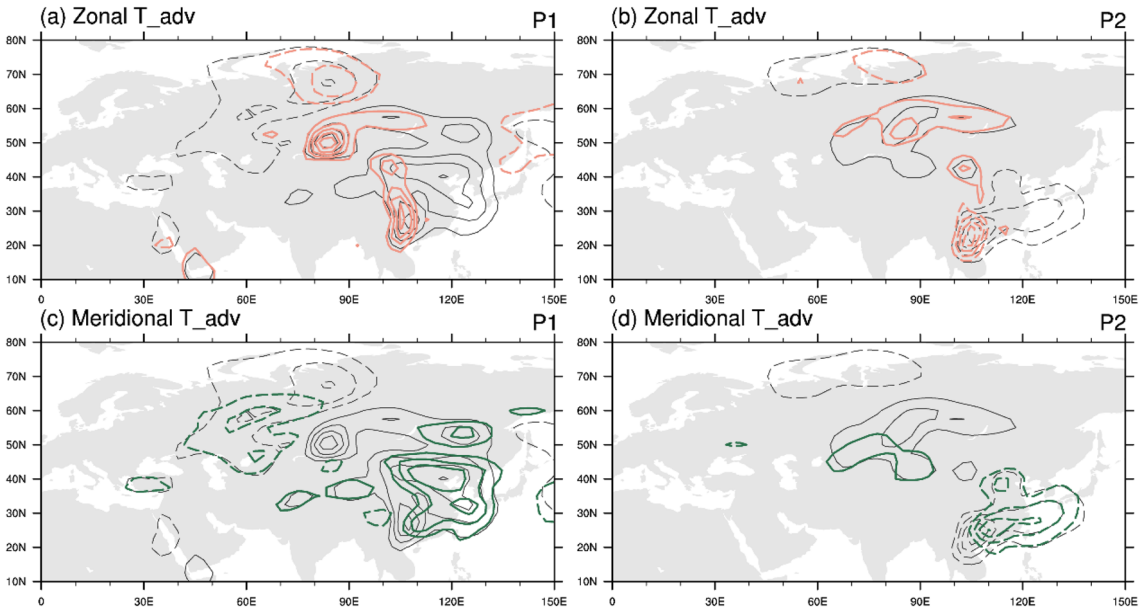

Fig. 10 Composite differences of **a**, **b** zonal (red contour) and meridional (green contour) temperature advection averaged from 850 to 300 hPa between days with positive (> 1.2 std) and negative (< − 1.2 std) **a**, **c** EAPJI_int in P1 and **b**, **d** EAPJI_loc in P2. Black contours represent total horizontal temperature advection. Solid and dashed lines denote positive and negative values, respectively

Based on the vertical distribution of thermal anomalies in the two subperiods (Fig. 10), two meridional temperature gradient indices (MTGI) relative to the major modes of EAPJ are introduced to affirm the thermal effects on the decadal ISV changes in EAPJ. The MTGI related to the leading mode (intensity change) of EAPJ in P1 (MTGI_M1) is defined by vertically averaging the area-mean meridional temperature gradients in region of (40°–60° N, 70°–120° E; green outline in Fig. 9c) from 850 hPa to 300 hPa. As shown in Fig. 11a, the variance of MTGI_M1 decreased visibly around 2000. Similarly, to define the MTGI associated with the leading mode (location shift) of EAPJ in P2 (MTGI_M2), the difference of the normalized meridional temperature gradient averaged over (40°–50° N, 70°–120° E; solid outline in Fig. 9d) and (52.5°–62.5° N, 70°–120° E; dashed outline in Fig. 9d) is calculated and then vertically averaged between 850 hPa and 300 hPa. As seen in Fig. 11b, the variance of MTGI_M2 increased significantly around 2000. It is therefore confirmed that the variability changes of the jet-related temperature gradients serve as a direct contribution to the ISV changes in EAPJ intensity and location around the year 2000.

Previous studies have reported that large-scale circulation in mid-high latitudes can be modulated by Arctic warming, which has been increasingly prominent since the twenty-first century (e.g. Berner et al. 2005; Francis and Vavrus 2012; Kug et al. 2015; Simpson et al. 2016). In particular, Francis and Vavrus (2012) proposed that Arctic warming can act to increase wave amplitude and weaken jet streams. Yet Simpson et al. (2016) argued that the zonal mean of subtropical jet has intensified under the warming background. Furthermore, some evidences have been presented concerning the effects of Arctic amplification on jet variabilities (Francis and Vavrus 2012, 2015; Woollings and Blackburn 2012; Barnes and Simpson 2017; Ronalds et al. 2018; Xu et al. 2018). It was espoused that rapid Arctic warming is related to increased occurrence frequency of high-amplitude jet streams (Francis and Vavrus 2015). Besides, the variability

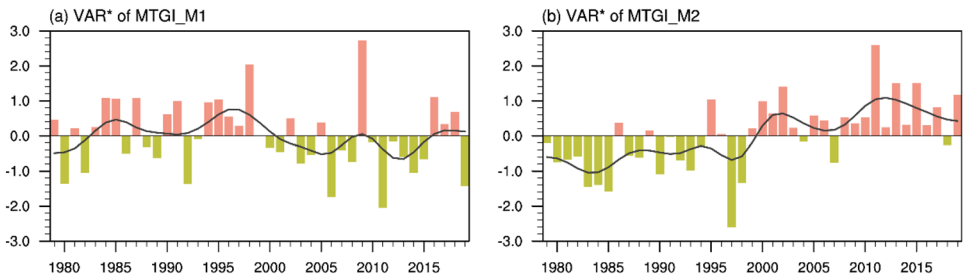

Fig. 11 Same as Fig. 2b, but for the meridional temperature gradient index related to **a** intensity change (MTGI_M1) and **b** location shift (MTGI_M2) of EPAJ

in zonal mean jet position was considered to decrease with Arctic amplification (Ronalds et al. 2018). Therefore, the possible role of Arctic warming in the decadal ISV changes of EAPJ is discussed in the following context.

To inspect the connection between Arctic warming and ISV changes in EAPJ, we compare the 1000–850-hPa vertically averaged temperature anomalies in the Arctic region relative to the dominant mode of EAPJ variation in the two subperiods (Fig. 12a, b). Note that 1000–850 hPa is selected because levels below 850 hPa show the most conspicuous amplification (Kaufman and Feldl 2022), and the anomalous temperature distribution within 1000–850 hPa is essentially the same as that at the surface (figure not shown). Apparent connection exists between the dominant mode of EAPJ variation and Arctic temperature anomalies in P1 especially near the Barents Sea with significant positive composite anomalies (Fig. 12a). However, such connection disappears in P2 (Fig. 12b). This decoupling of Arctic temperature and EAPJ variation may connote certain linkage between decadal changes in Arctic temperature anomalies and the dominant mode transition of EAPJ.

To delineate the decadal changes in Arctic air temperature, the lower-level temperature difference between the two subperiods is presented in Fig. 12c. It is seen that areas over the Barents Sea exhibits the most conspicuous warming trend. Therefore, the normalized mean and variance of temperature anomalies over Barents sector (72.5°–85° N, 0°–65° E; red outline in Fig. 12c) in each year are further displayed in Fig. 13. The mean temperature over Barents sector shows an evident uptrend and switches into a warm period around 2000 (Fig. 13a). By contrast, as revealed by the normalized variance over Barents sector (Fig. 13b), the Barents-temperature variability was decreased right after 2000, synchronous with the ISV changes of EAPJ. Such reverse decadal changes in the mean and variance of Arctic temperature are supported by previous studies, which

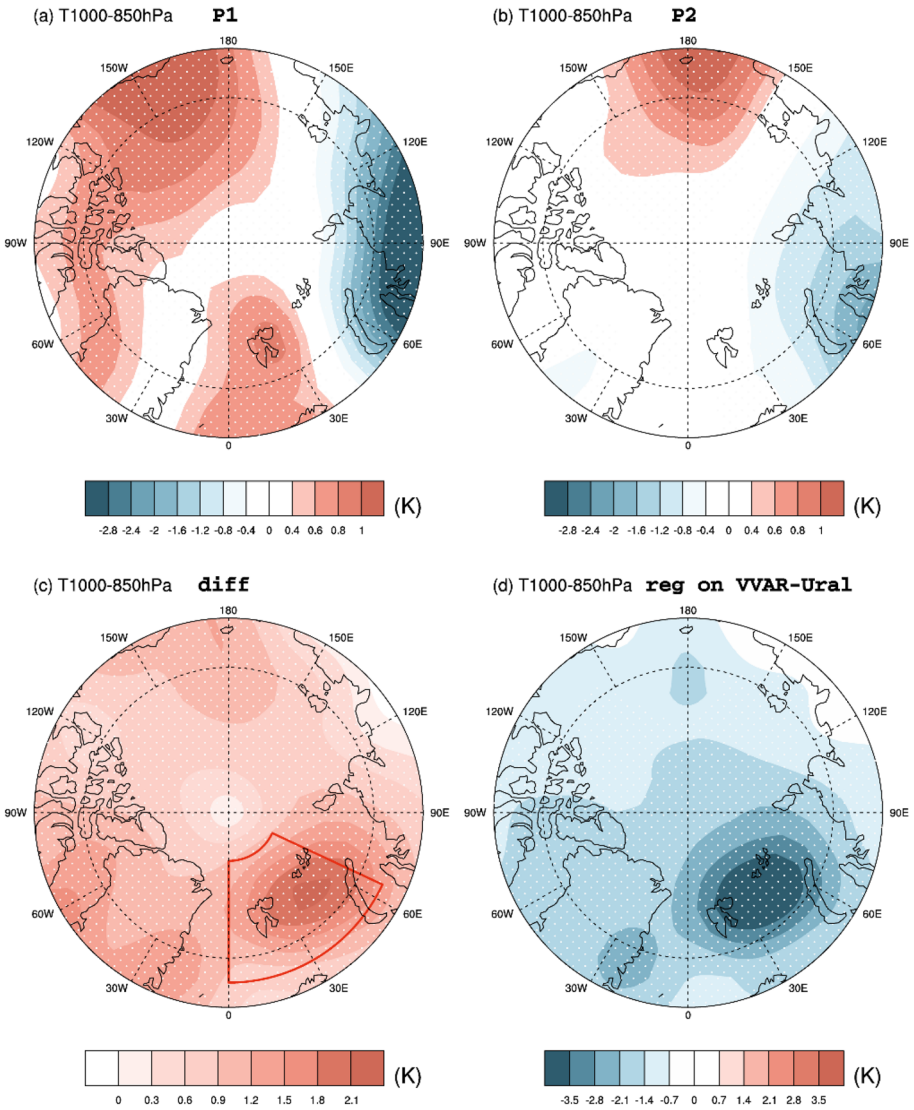

Fig.12 Composite anomalies of 1000–850 hPa vertically averaged daily temperature in Arctic regions between positive (> 1.2 std) and negative (< 1.2 std) **a** EAPJI_int in P1and **b** EAPJI_loc in P2. **c** The difference of 1000–850 hPa mean temperature between P2 and P1. **d** 1000–850 hPa mean temperature anomalies regressed against the decadal component of Ural-meridional wind variance. White dots indicate anomalies significant at 99% confidence level

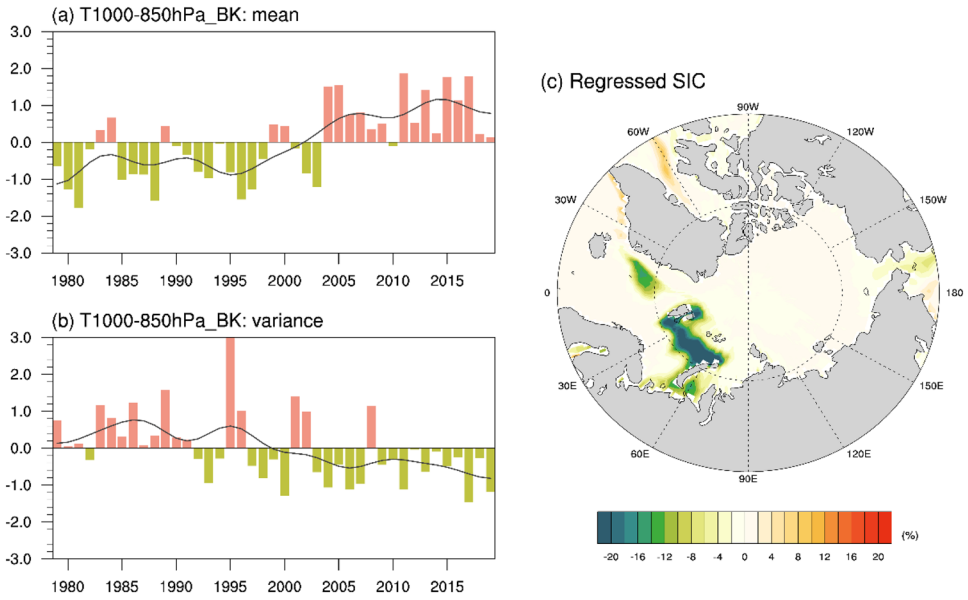

Fig. 13 Normalized **a** mean and **b** variance of 1000–850 hPa averaged daily air temperature anomalies over the Barents sector (72.5°–85° N, 0°–90° E) in each winter. **c** The regressed winter Arctic sea ice concentration (SIC) anomalies (%) against the normalized mean temperature series in the Barents sector

considered Arctic warming as effective in causing wavier and extreme weathers and altering subseasonal temperature variability in mid-high latitude regions (Francis and Vavrus 2012; Tang et al. 2013; Screen 2014; Xue et al. 2018; Dai and Deng 2021). Our research also noted a correlation of − 0.87 between the temperature mean and variance in Barents sector on decadal time scale (Table 1), which serves to support the close association between Arctic warming and temperature variability decreasing from a statistical point of view. The weakened temperature variability under Arctic warming has been mainly attributed to the role of meridional thermal advection (Screen 2014; Schneider et al. 2015; Chen et al. 2019; Collow et al. 2019; Tamarin-Brodsky et al. 2019; Dai and Deng 2021). For example, Screen (2014) found that northerly winds warm faster than southerly winds under Arctic amplification, which functions to weaken meridional heat advection. Collow et al. (2019) pointed out that the Arctic warming and sea ice loss can weaken the meridional temperature gradient as well as its variability, thereby reducing the temperature variability in turn. Dai and Deng (2021) further unraveled a positive feedback between temperature variability and meridional temperature advection under Arctic amplification. In general, the weakened magnitude of meridional heat advection plays a dominant role in decreasing the high-latitude temperature variability under global warming.

Relationships between these Arctic anomalies and EAPJ variabilities are also presented in Table 1. The mean temperature in Barents sector is correlated with the variance of EAPJI_int and EAPJI_loc at − 0.53 and 0.86, respectively. The temperature variance in Barents sector has correlations with EAPJI_int (0.56) and EAPJI_loc (− 0.87) almost equivalent to that of Barents temperature mean, but with opposite signs. The correlation between Barents temperature mean/variance and EAPJ variability validates the Arctic effects on East Asian jet variabilities.

As demonstrated before (Figs. 7c and 8a), the weakened variability of meridional winds in Ural region may be essential to the decadal changes in EAPJ variabilities. Then it is natural to ask if the weakened Ural-wind variability is connected to the Arctic temperature anomalies. To address this question, Fig. 12d further presents the Arctic temperature anomalies in winter regressed against the variance of Ural-meridional winds. Significant negative anomalies are observed in the Barents sector, indicating that Arctic warming, especially the Barents warming, can be effective in weakening the ISV of Ural-meridional winds. Moreover, also shown in Table 1, a correlation of − 0.69 (0.79) is detected between Barents temperature mean (variance) and Ural-meridional wind variance on decadal time scale. Such correlation in Urals proves to be the highest among Eurasian areas (Fig. 14), certifying that the Ural region is vital and irreplaceable in linking the Arctic temperature anomalies. These evidences demonstrate that the weakened Arctic temperature variability may prompt the variability decrease of Ural-meridional winds, which further induces the ISV changes of EAPJ. Therefore, the ISV decrease of Ural-meridional winds and the consequent Eurasian circulation adjustment can be deemed as a bridge that connects the Arctic anomalous temperature signals to EAPJ ISV changes.

The connection between Arctic temperature variations and Ural-meridional wind variability is sensible. As commonly known, wind tends to blow from cool to warm areas, and the larger the temperature difference is, the more strongly the wind blows. Conceivably, warmed Arctic temperature leads to weakened north–south temperature

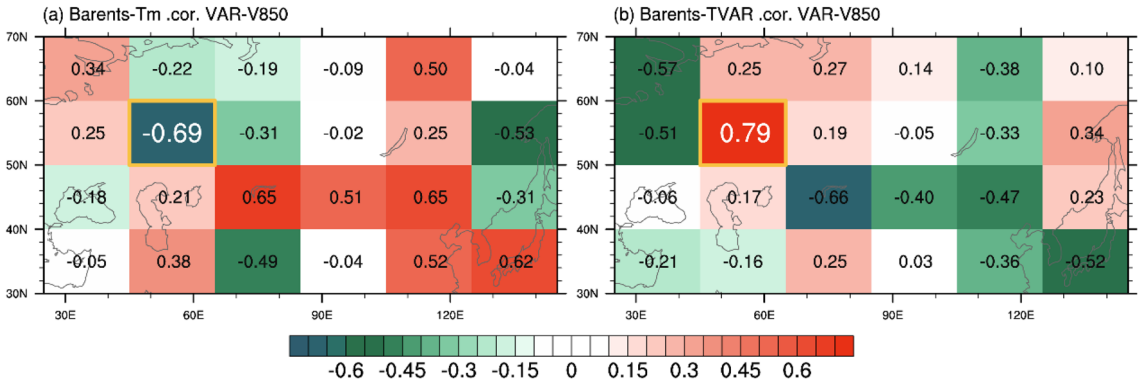

Fig. 14 **a** Correlation of Barents-temperature mean with the variance of intraseasonal meridional winds averaged in different regions of Eurasia. **b** Same as **a**, but of Barents-temperature variance. White text points out the Ural region where the coefficient bears the largest absolute value among all regions

difference, and decreased temperature variability alludes to strong cold winds intruding less frequently to mid-latitudes. Both cases are responsible to weakened cold-warm air mass interaction between the Arctic and mid-latitudes, particularly the Barents sector and the region to its south. As a consequence, the variability of the meridional wind in Ural region, which locates exactly at the south of the Barents sector, tends to witness apparent decrease. Additionally, a temperature difference index (TDI) is further applied to corroborate the weakening of air mass interaction between the two regions. TDI is defined as the difference between the temperature averaged in Barents and Ural. A weakened TDI variability should refer to decreased frequency of Arctic wind invasion. The variance of TDI shows an obvious downtrend, which changes the phase from positive to negative around 2000 (figure not shown). Therefore, it is implied that in the context of Arctic warming and temperature variability decreasing, the variability of temperature difference between Barents sector and Ural region is weakened, which benefits the variability decrease of Ural-meridional wind by weakening the north–south air mass interaction.

Many studies considered Arctic warming as affiliated with Arctic sea ice reduction (e.g. Kumar et al. 2010; Screen 2014; Ronalds et al. 2018; Ivasić et al. 2021). This affiliation can also be verified by the Arctic sea ice concentration (SIC) anomalies regressed against the normalized mean temperature over the Barents sector (Fig. 13b). Expectedly, remarkable negative anomalies are observed around the Barents Sea (Fig. 13c). In addition, there are also evidences directly supporting the impacts of Arctic sea ice reduction on mid- to high latitude atmospheric circulation including teleconnection patterns and wind fields (Alexander et al. 2004; Wu et al. 2011; Wu et al. 2013; Feldstein and Lee 2014; Ronalds et al. 2018; Yang et al. 2020; Li et al. 2021). For example, Wu et al. (2013) suggested that Arctic sea ice loss is dynamically coupled with the interdecadal variations of 850-hPa wind patterns over mid-high latitude Eurasia. Hence, the SIC is also regressed against the normalized total frequencies of extreme Ural-meridional winds to further certify the effects of Arctic sea ice loss (Fig. 8b). Notable positive SIC anomalies can be observed in the Barents Sea, suggesting that the Arctic sea ice loss may decrease the Ural-meridional wind variability by reducing the occurrences of extreme north–south wind oscillations. As further demonstrated in Fig. 8c–e, positive SIC anomalies can still be detected in Barents Sea in two months' leading, indicating that the Arctic SIC anomalies can lead the variability of Ural-meridional winds by around two months. These statistical analyses demonstrate that the Barents Sea ice loss may be construed as a potential external forcing on the decadal changes in the intraseasonal variations of EAPJ by modulating the associated circulation regimes over Eurasia.

6 Summary and discussions

Significant decadal changes in the intraseasonal variability (ISV) of East Asian jet stream are detected in this study. We find that the variance of intraseasonal zonal winds over East Asia (20°–70° N, 70°–120° E) decreased significantly around 2000. Further analysis demonstrates that the intraseasonal oscillation of East Asian westerlies is dominated by a period of 10–25 days, and is essentially dictated by the variability of East Asian polar front jet (EAPJ). The ISV of EAPJ abruptly changed around 2000 in both of its intensity and location. Specifically, the ISV of EAPJ intensity weakened after 2000, with the decrease in frequencies of both the extremely strong and weak cases. Meanwhile, the ISV of EAPJ location was enhanced, with the frequencies of extreme southward shifts increased more than that of extreme northward ones. In conjunction with the ISV changes, the leading mode of EAPJ intraseasonal variation

altered from its intensity change toward position shift around 2000.

The decadal ISV changes and mode transition of EAPJ are closely associated with the modulation of the large-scale circulation in lower troposphere over Eurasia. The ISV of meridional winds at 850 hPa over the Ural region was weakened significantly after 2000, which favors the transition in circulation patterns related to the dominant mode of EAPJ intraseasonal variations. In the earlier period (1979–1999; P1), when the Ural-meridional wind variability is stronger, Arctic cold air mass can invade deep into southern Eurasia, inspiring a cyclonic anomaly overriding the whole Eurasian continent. By contrast, the meridional wind variability is evidently weakened in the recent period (2000–2019; P2). Therewith, the northerly winds over the Ural region are debilitated at mid-latitude Eurasia around 50° N, narrowing down the cyclonic anomaly and generating a meridional dipole with elongated cyclonic and anticyclonic anomalies over mid-high latitude and subtropical Eurasia, respectively. The distinct circulation patterns in lower troposphere in the two subperiods further result in differences in temperature distribution and its meridional gradient over East Asia, mainly through the effect of both the zonal and meridional temperature advection, and these different temperature gradient patterns then favor different EAPJ variation modes via thermal wind relation. Coinstantaneous variability changes can be additionally detected around 2000 in the temperature gradients associated with EAPJ's intensity and location variations, further underpinning the thermal effects on the decadal ISV changes of EAPJ.

The modulation of mid-high latitude circulation and temperature distribution are further linked to Arctic temperature anomalies. The temperature over the Barents sector has warmed remarkably since 2000, with its variability weakened synchronously. The Barents-temperature anomalies are well correlated with that of Ural-meridional winds on decadal time scale. Such correlation imply that the weakened Arctic temperature variability may suppress the meridional oscillation of Ural winds and further conduce to the EAPJ-related circulation changes, probably by weakening the cold-warm air mass interaction between the Arctic and mid-high latitudes. Moreover, based on statistical analysis, the Arctic warming and decreased variability of Ural-meridional winds are both related to the sea ice reduction in the Barents Sea, and the Barents Sea ice anomalies can lead the Ural-meridional wind variability for around two months. These evidences indicate that the Barents Sea ice loss may be a potential external forcing of the decadal transitions in the ISV of EAPJ.

The existing literatures seemingly have not reached a consensus upon interdecadal trends of jet variabilities associated with sea ice loss and Arctic amplification. On the one side, the increased (decreased) ISV of EAPJ location (intensity) in our results is physically espoused by studies of Francis and Vavrus (2012, 2015). They reported that Arctic amplification gives rise to wavier flows and weaker zonal winds, which can be instrumental for larger amplitudes in latitudinal shifts of EAPJ yet unfavorable for its overall strength change. Nonetheless, weakened positional variability of zonal mean eddy-driven jet was simulated with imposed Arctic heating by Ronalds et al. (2018) using a dry core coupled general circulation models (GCM). Besides, Xu et al. (2018) identified accelerated EASJ in December and decelerated EASJ in following January and February in a low-SIC boreal winter (2014/2015), which implicates enhanced variability in EASJ intensity on an intraseasonal time scale of 30–60 days. We assume these discrepancies might stem from disparities in time scales and domains of concern among these literatures. From another point, such discrepancies also highlight a necessity to separately analyze the unique variability of the two East Asian jets. More effects deserve to be devoted to relevant issues.

Other than the influence from Arctic, thermal forcings from tropics and subtropics, such as forcings from sea surface of Atlantic and Pacific Ocean as well as Tibetan Plateau snow cover, may well play a role in the ISV changes of the jets (Wu and Liu 2016; Huang et al. 2019; Xiao et al. 2020a, b). As a matter of fact, our preliminary examination has revealed that the effects of sea surface temperature (SST) in the Pacific also plays a part. As exhibited in Fig. 15a, b, SST anomalies regressed on the variance of EAPJ indices, particularly those regressed on variance of the EAPJ location shift index (EAPJI_loc) (Fig. 15b), resemble the Interdecadal Pacific Oscillation (IPO). IPO index has been unveiled to undergo a phase shift generally around 2000 (Dai 2013; Huang et al. 2019), and is correlated with the variance of EAPJI_int (EAPJI_loc) at − 0.47 (0.83) on decadal time scale according to our examination. Moreover, the SST anomalies regressed on variance of meridional temperature gradient indices (MTGI) are also akin to IPO pattern (Fig. 15c, d). Hence, it can be preliminary inferred that the IPO may also contribute to the intraseasonal mode transition of EAPJ, especially to amplifying the variability of EAPJ location shift, through regulating the temperature gradients over East Asia.

Besides, dynamical processes like interactions between basic flow and synoptic/low-frequency transient eddies should also be non-negligible (Lorenz and Hartmann 2003; Ding and Wang 2007; Ren et al. 2010; Chowdary et al. 2019). In fact, we have found that both of the Eurasian wave trains associated with the intensity and location variation of EAPJ underwent consistent decadal changes in

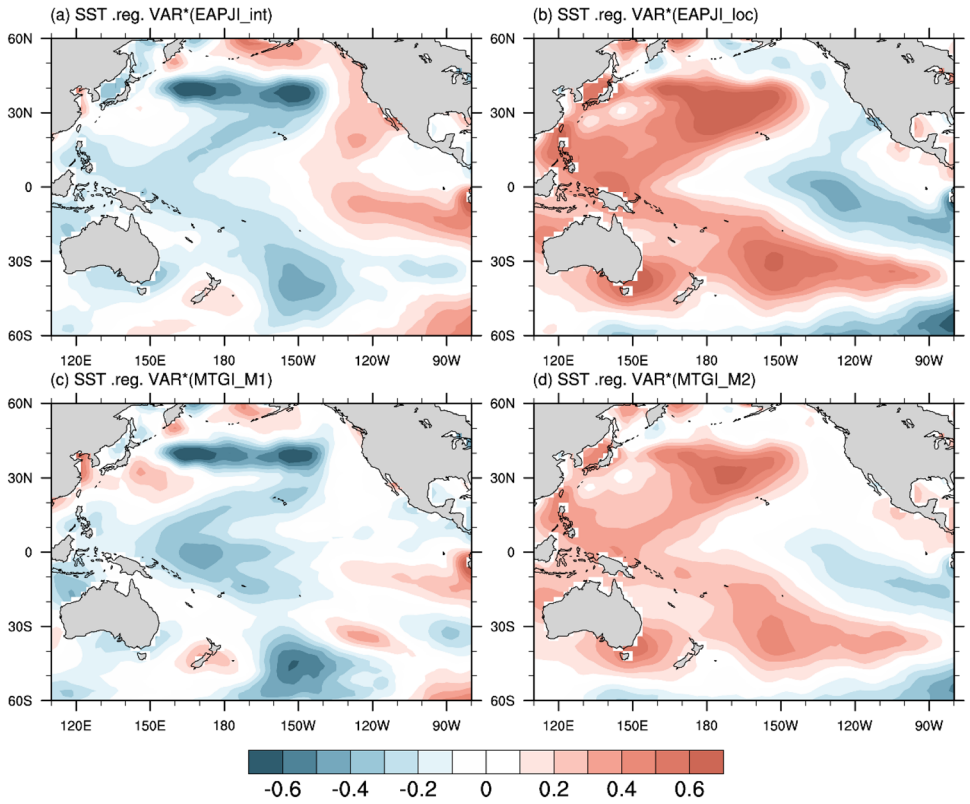

Fig. 15 SST anomalies regressed against the decadal variance of **a** EAPJI_int, **b** EAPJI_loc, **c** MTGI_M1 and **d** MTGI_M2 in Pacific region

amplitude around 2000, indicating that Eurasian teleconnections may also conduce to the decadal ISV changes of EAPJ. In view of the limitation of paper length, we will provide more detailed and comprehensive results upon this issue in future works.

In this research, examination begins with the variance detection of East Asian mean intraseasonal zonal wind, instead of an EOF analysis of zonal wind in East Asia as commonly supposed. This method is unadopted because it works less effectively in capturing the decadal ISV changes of East Asian jets (figure not shown). The involvement of EASJ possibly accounts for such dissatisfactory results, yet it can be hardly separated out. Even so, EOF analysis confined to EAPJ key region can help boost confidence in the decadal ISV changes in EAPJ intensity and location. As is shown in Fig. 16, the first two EOF modes of EAPJ during 1979–2019 feature its intensity and location variation. EOF1 represents the EAPJ intensity change (Fig. 16a), which is almost the same as EOF1 in P1 (Fig. 4a). Correspondingly, the variance of PC1 can also display a clear decrease around 2000 (Fig. 16c), exactly consistent with the variance of EAPJI_int (Fig. 2b). EOF2 denotes the EAPJ location shift (Fig. 16b), showing a pattern quite similar to EOF1 in P2 (Fig. 4b) but slightly northward shifted in comparison. The variance of PC2 does not show as clear a decadal change as that of EAPJI_loc (Fig. 5), but still exhibits an evident uptrend which intersects the zero line right at 2000 (Fig. 16d). Such decadal evolution of PC variances ensures the robustness of the decadal ISV changes of EAPJ.

As a rule, coincident relationship can be expected between the variability and occurrence probability of extreme cases for certain variables. Our research shows consistent results that the decadal ISV transitions in East Asian jet stream hinge much on the changes in extreme cases of jet intensity/location. We also notice that close connection between the intraseasonal jet variations and frequencies of extreme climate anomalies on decadal time scale has been implicated in previous studies (Woo et al. 2012; Kuang et al. 2016; Ronalds et al. 2018; Zhu et al. 2022). Particularly, the decadal ISV changes of East Asia jet stream seem to bear good synchronization with those of extreme cold events (Woo et al. 2012; Kuang et al. 2016). We did not extendedly discuss this topic in the present paper to keep the paper reasonably concise, but pertinent future examination is worthy of conduction.

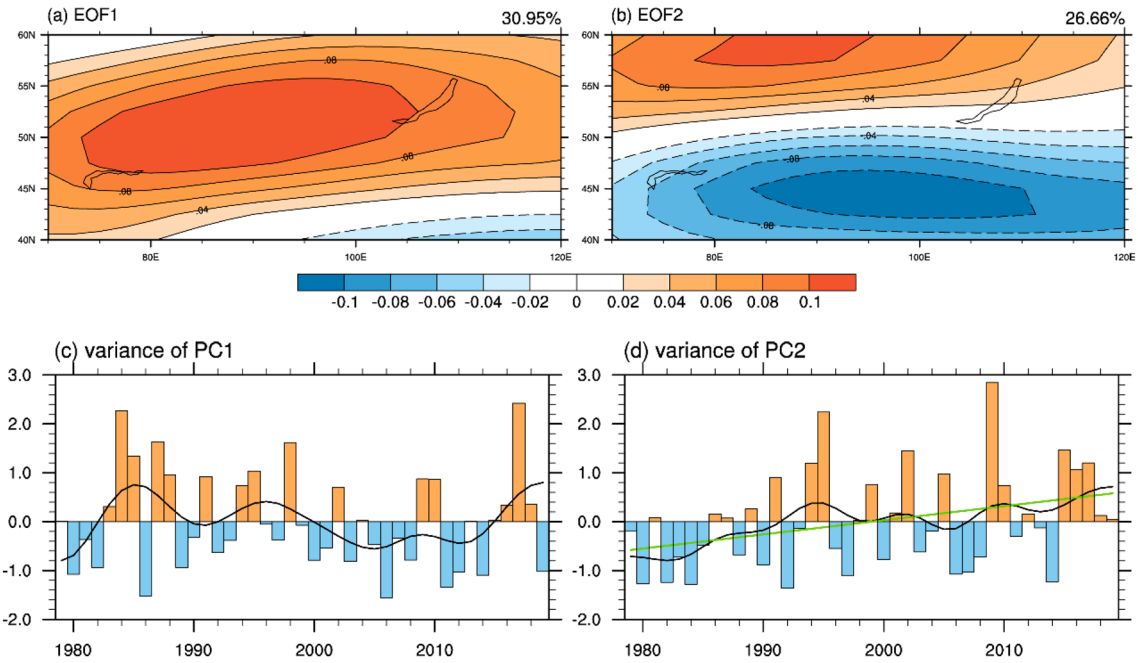

Fig. 16 **a**, **b** EOF analysis of 10–25-day filtered 300-hPa zonal wind in EAPJ key region (40°–60° N, 70°–120° E) from 1979 to 2019. **c**, **d** Normalized variance of corresponding PCs in each year. Black line in **c**, **d** denotes decadal component of the normalized variance

Acknowledgements We thank the editor Prof. Li and three anonymous reviewers for constructive comments that helped improve the quality of the manuscript. This work was supported by the National Natural Science Foundation of China (Grant 41930969 and 42105051).

Funding This article is funded by Key Programme(41930969).

Data availability All NCEP Reanalysis data are obtained from NOAA/OAR/ESRLPSD at https://psl.noaa.gov/data/gridded/data.ncep.reanalysis.html. Sea ice concentration (SIC) data are provided by the Met Office Hadley Center which can be downloaded from https://www.metoffice.gov.uk/hadobs/hadisst/data/download.html. SST data can be derived from https://www.esrl.noaa.gov/psd/data/gridded/data.noaa.ersst.v5.html.

Declarations

Conflict of interest The authors declare that they have no known competing financial interests or personal relationships that could have appeared to influence the work reported in this paper.

References

Alexander MA, Bhatt US, Walsh JE et al (2004) The atmospheric response to realistic Arctic sea ice anomalies in an AGCM during winter. J Clim 17:890–905

Athanasiadis PJ, Wallace JM (2010) Patterns of wintertime jet stream variability and their relation to the storm tracks. J Atmos Sci 67:1361–1381

Barnes EA, Simpson IR (2017) Seasonal sensitivity of the Northern Hemisphere jet streams to Arctic temperatures on subseasonal time scales. J Clim 30:10117–10137

Berner J et al (2005) Arctic climate impact assessment. Cambridge University Press, Cambridge, p 1042

Chen W, Lu RY (2014) A decadal shift of summer surface air temperature over Northeast Asia around the mid-1990s. Adv Atmos Sci 31:735–742

Chen Y, Zhai PM (2014) Two types of typical circulation pattern for persistent extreme precipitation in Central-Eastern China. Q J R Meteorol Soc 140:1467–1478

Chen JP, Wen ZP, Wu RG et al (2015) Influences of northward propagating 25–90-day and quasi-biweekly oscillations on eastern China summer rainfall. Clim Dyn 45:105–124

Chen JP, Wen ZP, Wu RG et al (2017) An interdecadal change in the intensity of interannual variability in summer rainfall over southern China around early 1990s. Clim Dyn 48:191–207

Chen J, Dai AG, Zhang YC (2019) Projected changes in daily variability and seasonal cycle of near-surface air temperature over the globe during the twenty-first century. J Clim 32:8537–8561

Chen RD, Wen ZP, Lu RY et al (2021) Interdecadal changes in the interannual variability of the summer temperature over Northeast Asia. J Clim 34:8361–8376

Cheng YF et al (2020) Causes of interdecadal increase in the intraseasonal rainfall variability over Southern China around the early 1990s. J Clim 33:9481–9496

Chowdary JS et al (2019) The Eurasian jet streams as conduits for East Asian monsoon variability. Curr Clim Chang Reports 5:233–244

Cohen J et al (2014) Recent Arctic amplification and extreme mid-latitude weather. Nat Geo 7:627–637

Collow TW, Wang WQ, Kumar A (2019) Reduction in northern mid-latitude 2-m temperature variability due to Arctic sea ice loss. J Clim 32:5021–5035

Dai AG (2013) The influence of the inter-decadal Pacific oscillation on US precipitation during 1923–2010. Clim Dyn 41:633–646
Dai AG, Deng JC (2021) Arctic amplification weakens the variability of daily temperatures over northern middle-high latitudes. J Clim 34:2591–2609
Deng Y, Jiang TY (2011) Intraseasonal modulation of the North Pacific storm track by tropical convection in boreal winter. Clim Dyn 24:1122–1137
Ding QH, Wang B (2007) Intraseasonal teleconnection between the summer Eurasian wave train and the Indian Monsoon. J Clim 20:3751–3767
Duchon CE (1979) Lanczos filtering in one and two dimensions. J Appl Meteorol 18:1016–1022
Feldstein SB, Lee S (2014) Intraseasonal and interdecadal jet shifts in the Northern Hemisphere: the role of warm pool tropical convection and sea ice. J Clim 27:6497–6518
Francis JA, Vavrus SJ (2012) Evidence linking Arctic amplification to extreme weather in mid-latitudes. Geophys Res Lett 39
Francis JA, Vavrus SJ (2015) Evidence for a wavier jet stream in response to rapid Arctic warming. Environ Res Lett 10:014005
Gilman D, Fuglister F, Mitchell J (1963) On the power spectrum of "red noise." J Atmos Sci 20:182–184
Hong CC, Hsu HH, Chia HH (2009) A study of East Asian cold surges during the 2004/05 winter: impact of East Asian Jet stream and subtropical upper-level Rossby wave trains. Terr Atmos Ocean Sci 2:3
Hoskins BJ, James IN, White GH (1983) The shape, propagation and mean-flow interaction of large-scale weather systems. J Atmos Sci 40:1595–1612
Hu KM, Hunag G, Wu RG et al (2018) Structure and dynamics of a wave train along the wintertime Asian jet and its impact on East Asian climate. Clim Dyn 51:4123–4137
Huang DQ, Zhu J, Zhang YC et al (2015) The impact of the East Asian subtropical jet and polar front jet on thefrequency of spring persistent rainfall over southern China in 1997–2011. J Clim 28:6054–6066
Huang DQ, Dai AG, Zhu J et al (2017) Recent winter precipitation changes over Eastern China in different warming periods and the associated East Asian jets and oceanic conditions. J Clim 30:4443–4462
Huang DQ, Dai AG, Yang B et al (2019) Contributions of different combinations of the IPO and AMO to recent changes in winter East Asian jets. J Clim 32:1607–1626
Ito H, Johnson HC, Xie SP (2013) Subseasonal and interannual temperature variability in relation to extreme temperature occurrence over East Asia. J Clim 26:9026–9042
Ivasić S, Herceg-Bulić I, King MP (2021) Recent weakening in the winter ENSO teleconnection over the North Atlantic-European region. Clim Dyn 57:1953–1972
Jaffe SC, Martin JE, Vimont DJ et al (2011) A synoptic climatology of episodic, subseasonal retractions of the Pacific jet. J Clim 24:2846–2860
Kalnay E, Higgins W, Janowiak J et al (1996) The NCEP/NCAR 40-year reanalysis project. Bull Am Meteorol Soc 77:737–771
Kaufman ZS, Feldl N (2022) Causes of the Arctic's lower-tropospheric warming structure. J Clim 35:1983–2002
Kosaka Y, Nakamura H (2006) Structure and dynamics of the summertime Pacific–Japan teleconnection pattern. Q J R Meteorol Soc 132(619):2009–2030. https://doi.org/10.1256/qj.05.204
Kuang XY, Zhang YC (2005) Seasonal variation of the East Asian Subtropical Westerly Jet and its association with the heating field over East Asia. Adv Atmos Sci 22:831–840
Kuang XY, Zhang YC, Huang Y et al (2014) Changes in the frequencies of record-breaking temperature events in China and its association with East Asian Winter Monsoon variability. J Geophys Res Atmos 119:1234–1248
Kuang XY, Zhang YC, Huang DQ et al (2016) Regionality of record-breaking low temperature events in China and its associated circulation. Clim Dyn 46:1719–1731
Kug JS, Jeong JH, Jang YS et al (2015) Two distinct influences of Arctic warming on cold winters over North America and East Asia. Nat Geosci 8:759–762
Kumar A, Perlwitz J, Eischeid J et al (2010) Contribution of sea ice loss to Arctic amplification. Geophys Res Lett 37:L21701
Lee S, Feldstein SB (2013) Detecting ozone- and greenhouse-gas-driven wind trends with observational data. Science 339:563–567
Li L, Zhang YC (2014) Effects of different configurations of the East Asian subtropical and polar front jets on precipitation during the Mei-yu season. J Clim 27:6660–6672
Li KP, Yang Y, Feng L et al (2020) Structures and northward propagation of the quasi-biweekly oscillation in the western north pacific. J Clim 33:6873–6888
Li MY, Luo DH, Simmonds I et al (2021) Anchoring of atmospheric teleconnection patterns by Arctic Sea ice loss and its link to winter cold anomalies in East Asia. Int J Climatol 41:547–558
Liao ZJ, Zhang YC (2013) Concurrent variation between the East Asian subtropical jet and polar front jet during persistent snowstorm period in 2008 winter over southern China. J Clim 118:6360–6373
Lorenz D, Hartmann D (2003) Eddy-zonal flow feedback in the Northern Hemisphere winter. J Clim 16:1212–1227
Luo X, Zhang YC (2015) The linkage between upper-level jet streams over East Asia and East Asian Winter Monsoon variability. J Clim 28:9013–9028
Matthews AJ, Kiladis GN (1999) The tropical-extratropical interaction between high-frequency transients and the Madden–Julian oscillation. Mon Weather Rev 127:661–677
Rayner NA, Parker DE, Horton EB et al (2003) Global analyses of sea surface temperature, sea ice, and night marine air temperature since the late nineteenth century. J Geophys Res Atmos 108:4407
Ren XJ, Yang XQ, Chu CJ (2010) Seasonal variations of the synoptic-scale transient eddy activity and polar front jet over East Asia. J Clim 23:3222–3233
Robinson DP, Black RX (2005) The statistics and structure of subseasonal midlatitude variability in NASA GSFC GCMs. J Clim 18:3294–3316
Ronalds B, Barnes E, Hassanzadeh P (2018) A barotropic mechanism for the response of Jet Stream variability to arctic amplification and sea ice loss. J Clim 31:7069–7085
Schneider T, Bischoff T, Plotka H (2015) Physics of changes in synoptic midlatitude temperature variability. J Clim 28:2312–2331
Screen JA (2014) Arctic amplification decreases temperature variance in northern mid- to high-latitudes. Nat Clim C 4:577–582
Serreze MC, Barrett AP, Stroeve JC et al (2009) The emergence of surface-based Arctic amplification. J Cryos 3:11–19
Shen HY, Zhao JH, Cheung KY et al (2021) Causes of the extreme snowfall anomaly over the northeast Tibetan plateau in early winter 2018. Clim Dyn 56:1767–1782
Simpson IR, Seager R, Ting MF, Shaw TA (2016) Causes of change in Northern Hemisphere winter meridional winds and regional hydroclimate. Nat Clim Chang 6:65–71
Song L, Wu RG (2018) Comparison of intraseasonal East Asian winter cold temperature anomalies in positive and negative phases of the Arctic oscillation. J Geophy Res Atmos 123:8518–8537
Song L, Wang L, Chen W et al (2016) Intraseasonal variation of the strength of the East Asian trough and its climatic impacts in boreal winter. J Clim 29:2557–2577
Tamarin-Brodsky T, Hodges K, Hoskins BJ et al (2019) A dynamical perspective on atmospheric temperature variability and its response to climate change. J Clim 32:1707–1724
Tanaka S, Nishii K, Nakamura H (2016) Vertical structure and energetics of the western Pacific teleconnection pattern. J Clim 29:6597–6616

Tang QH, Zhang XJ, Yang XH et al (2013) Cold winter extremes in northern continents linked to Arctic sea ice loss. Environ Res Lett 8:014036

Wang L, Chen W (2014) The East Asian winter monsoon: re-amplification in the mid-2000s. Chin Sci Bull 59:430–436

Wang N, Zhang YC (2015) Connections between the Eurasian teleconnection and concurrent variation of upper-level jets over East Asia. Adv Atmos Sci 32:336–348

Wei K, Chen W (2011) An abrupt increase in the summer high temperature extreme days across China in the mid-1990s. Adv Atmos Sci 28:1023–1029

Woo SH, Kim BM, Jeong JH et al (2012) Decadal changes in surface air temperature variability and cold surge characteristics over northeast Asia and their relation with the Arctic Oscillation for the past three decades (1979–2011). J Geophy Res Atmos 117(D18)

Woollings T, Blackburn M (2012) The north Atlantic jet stream under climate change and its relation to the NAO and EA patterns. J Clim 25:886–902

Wu GX, Liu YM (2016) Impacts of the Tibetan Plateau on Asian climate. Meteorol Monogr 56:7.1-7.29

Wu BY, Su JZ, Zhang RH (2011) Effects of autumn-winter Arctic sea ice on winter Siberian High. Chin Sci Bull 56:3220–3228

Wu BY, Handorf D, Dethloff K et al (2013) Winter weather patterns over northern Eurasia and arctic sea ice loss. Mon Weather Rev 141:3786–3800

Xiao HX, Zhang F, Miao LJ et al (2020a) Long-term trends in Arctic surface temperature and potential causality over the last 100 years. Clim Dyn 55:1443–1456

Xiao XC et al (2020b) Contributions of different combinations of the IPO and AMO to the concurrent variations of summer east Asian jets. J Clim 33:7967–7982

Xu XP et al (2018) Subseasonal reversal of East Asian surface temperature variability in winter 2014/15. Adv Atmos Sci 35:737–752

Xue DK, Zhang YC (2017) Concurrent variations in the location and intensity of the Asian winter jet streams and the possible mechanism. Clim Dyn 49:37–52

Xue DK, Lu J, Sun LT, Chen G, Zhang YC (2018) Local increase of anticyclonic wave activity over northern Eurasia under amplified arctic warming. Geophys Res Lett 44:3299–3308

Yang XY, Zeng G, Zhang GW, Li ZX (2020) Interdecadal variation of winter cold surge path in east Asia and its relationship with arctic sea ice. J Clim 33:4907–4925

Yao CY et al (2018) The 10–30-day oscillation of winter zonal wind in the entrance region of the East Asian subtropical jet and its relationship with precipitation in southern China. Dyn Atmos Ocean 82:76–88

Yin JN, Zhang YC (2021) Decadal changes of East Asian jet streams and their relationship with the mid-high latitude circulations. Clim Dyn 56(9):2801–2821

You YJ, Ting MF (2021) Low pressure systems and extreme precipitation in Southeast and East Asian monsoon regions. J Clim 34:1147–1162

Zhang YC et al (2006) Seasonal evolution of the upper-tropospheric westerly jet core over East Asia. Geophys Res Lett 33(11)

Zhang M, Qi Y, Hu XM (2014) Impact of East Asian winter monsoon on the Pacific storm track. Meteorol Appl 21:873–878

Zhou BT, Wang ZY, Sun B et al (2021) Decadal change of heavy snowfall over Northern China in the mid-1990s and associated background circulations. J Clim 34:825–837

Zhu BY, Sun B, Wang HJ (2022) Increased interannual variability in the dipole mode of extreme high-temperature events over East China during summer after the early 1990s and associated mechanisms. J Clim 35:1347–1364